ISSN 2306-5478

УДК 621.865:615.47 https://doi.org/10.31713/vt3202515

Tys M. A. [1; ORCID ID: 0009-0004-2208-9103],
Post-graduate Student,
Korendii V. M. [1; ORCID ID: 0000-0002-6025-3013],
Candidate of Engineering (Ph.D.), Associate Professor,
Markovych B. M. [1; ORCID ID: 0000-0002-8813-9108],
Doctor of Physical and Mathematical Sciences, Professor,
Vyshnevskyi O. I. [1; ORCID ID: 0009-0006-7648-8630],
Post-graduate Student

[1]*Lviv Polytechnic National University, Lviv, Ukraine*

KINEMATIC AND FORCE ANALYSIS OF THE PELVIS-FOOT SECTION OF AN EXOSKELETON FOR THE REHABILITATION OF INDIVIDUALS WITH MUSCULOSKELETAL DISORDERS

This study presents a kinematic and force analysis of the pelvis–foot section of a passive lower-limb exoskeleton aimed at assisting the rehabilitation of individuals with musculoskeletal disorders. The architecture features a two-segment foot linked by a cylindrical hinge with a rubber outsole, shank and thigh links, a pelvic plate, and energy-storing spring-damper modules positioned at the ankle, knee, and hip. In the unloaded configuration, the segments are set to a quasi-physiological arrangement (e.g., a 120–140° foot-shank angle); during the sit-to-stand cycle the elastic modules accumulate and release energy to reduce user effort. The kinematic model employs a closed-vector-loop formulation for a planar three-link chain with three generalized coordinates; numerical trajectories are generated in MathCad software using a two-stage timing profile (total cycle duration of 2 s). A MapleSim multibody model is developed to validate the analytical motion laws, confirming characteristic paths: a circular knee locus about the ankle, an elliptic hip trajectory, and a controlled trunk lean-and-recovery. The load analysis considers vertical static loading and the transition to bending during sitting; the thigh link, as a critical member, is evaluated by finite-element analysis in SolidWorks Simulation software. The maximum equivalent stress is approximately 154 MPa with a tip deflection not exceeding 0.3 mm under design load up to 1.5 kN, satisfying the strength criterion for steel St. 3 (with allowable stress of about160 MPa). Overall, the proposed design and the parameterization of the spring-damper units are sufficient to assist sit-to-stand motions and provide a sound basis for subsequent optimization to user anthropometrics and rehabilitation protocols.

Keywords: passive exoskeleton; rehabilitation; kinematics; force

analysis; method of closed vector loops; MathCad; MapleSim; SolidWorks Simulation; finite-element analysis; spring-damper unit; pelvis-foot segment.

1. Introduction. Musculoskeletal impairments limit fundamental motor functions – most notably sit-to-stand, stance stabilization, and gait initiation. Lower-limb exoskeletons are promising rehabilitation tools because they can redistribute loads along the hip-knee-ankle-foot chain, guide joint motion, and provide assistance without heavy actuators. The pelvis-foot section is pivotal: it governs ground interaction, sets pelvic alignment, and largely defines the kinematic and load conditions for the entire device.

Key engineering challenges remain tightly coupled: aligning artificial joints with anatomical axes, preserving physiologic ranges of motion, selecting and locating spring-damper elements, and minimizing mass while maintaining stiffness and safety. Insufficiently resolved trade-offs at this level lead to peak-load amplification, user discomfort, and degraded motion quality.

There is a need for quantitative relations that link the geometry and passive module parameters of the pelvis-foot section to: 1) the kinematics of representative rehabilitation tasks (primarily sit-to-stand); 2) the distribution of internal/external forces and joint reactions; 3) performance and comfort constraints (limits on angles, velocities, and peak loads).

The objective of further investigations on the subject of this paper is to develop a generalized kinematic and force model of the pelvis-foot segment of a passive lower-limb exoskeleton and, based on it, assess how design parameters shape motion trajectories and structural loading under typical rehabilitation scenarios. The outcomes are intended to provide design guidelines for choosing stiffness/damping, pretension, and geometry, and for strength checks of critical members.

2. Background and Related Work. Lower-limb exoskeletons have advanced rapidly over the past decade as rehabilitation tools for people with musculoskeletal and neuromotor impairments. Recent systematic reviews report a growing clinical uptake, but also emphasize unresolved questions about the optimal device architecture, assistance strategy, and training dosage for functional tasks beyond level walking – especially sit-to-stand (STS) and stand-to-sit transfers that dominate daily living [1; 2]. These surveys span clinical outcomes and control approaches and collectively conclude that assistance must be tuned to

 ISSN 2306-5478

task biomechanics and human-device interaction (HDI) constraints to be effective [3].

The STS maneuver is a compact but demanding multi-joint action with substantial hip and knee extensor moments and a coordinated forward trunk lean for momentum generation [4]. Classic studies show that increasing ascent speed elevates peak resultant joint torques at the hip, knee, and ankle, underscoring the need for devices that modulate load paths without provoking compensations [5]. Determinants such as seat height, foot placement, and use of armrests strongly influence joint moments and strategy selection, while trunk kinematics and spinal motion patterns further affect perceived effort and balance [6]. Disease and surgery alter these mechanics: e.g., post-arthroplasty patients display modified STS strategies that shift demand across joints [7]. These observations motivate exoskeleton sections that span pelvis to foot, where pelvis alignment and foot-ground interaction jointly set the feasible kinematic envelope and reaction forces during transfers [8].

Recent analyses refine these insights with 3-D motion capture and model-based approaches, quantifying healthy STS trajectories and phase timing, and reinforcing that design choices which restrict sagittal plane motion or misalign joint axes can amplify internal loads [9]. Age-related neuromechanical changes (e.g., reduced power generation and altered coordination) further justify passive assistance focused on hip-knee extension with controlled ankle and trunk synergy [10].

Powered exoskeletons can substantially reduce metabolic cost in locomotion when torque timing and magnitude are optimized across hip, knee, and ankle; however, their weight, cost, and control complexity pose barriers in rehabilitation contexts emphasizing safety, portability, and ease of donning [11]. Optimization studies demonstrate speed-dependent allocation of assistance and highlight relatively small ankle torques at slow walking speeds, suggesting that for slow, transitional tasks (like STS) passive or quasi-passive strategies may be preferable.

At the ankle and ankle-foot, powered devices have achieved meaningful metabolic reductions during walking, yet transfer these benefits inconsistently to non-cyclic tasks [12; 13]. Conversely, quasi-passive and passive designs – leveraging springs, clutches, and dampers – store and release energy with minimal added mass and have shown efficiency gains and reduced muscular demand in level gait and squat-like activities, offering a promising template for STS assistance [14; 15].

Evidence specific to STS is emerging. A fully soft passive "knee-assist wear" reduced effort during STS through elastic energy return [16]; clinical pilot work with thigh-assist exosuits in geriatric cohorts indicates feasible support and improved transfer performance [17]; and recent mechanism/kinetic models for knee-assist exoskeletons explicitly target sit-to-stand/stand-to-sit, informing design parameterization for torque-angle profiles and energy exchange [18]. Together, these studies point to the value of passive or quasi-passive modules tuned to the characteristic joint excursions of STS.

A recurring limitation across wearable robots is joint misalignment between human anatomy and device hinges, which induces parasitic torques and shear forces, degrading comfort and increasing internal joint loads [19]. Foundational reviews and experimental studies demonstrate that even millimetric offset can inflate knee contact forces during swing and stance, while dedicated mechanisms at the hip (three rotational DOFs, self-aligning linkages) mitigate these penalties without sacrificing range of motion [20]. Newer designs explore adaptive knee joints that treat the human limb as part of the mechanism, reducing relative motion at the interface [21; 22]. These results directly motivate careful synthesis of pelvis–hip assemblies and foot modules in a pelvis–foot exoskeleton section, where alignment governs both kinematic compatibility and the path of ground reaction forces [23].

At the distal end, ankle and foot assistance substantially shape overall limb mechanics. Soft ankle exoskeletons for drop-foot have normalized ankle/foot kinematics in gait tests, and parametric work on exoskeleton timing/power shows measurable effects on gait variability – implicating the importance of ankle-foot module timing and compliance for stability during transitional tasks [24]. Although these studies target locomotion, their control-independent lessons (foot clearance, inversion control, rocker dynamics) transfer directly to STS, where foot segmentation and outsole compliance can regulate COM shift and peak loading [25].

From a rehabilitation perspective, dosing matters as much as mechanism. A recent systematic review of overground exoskeleton training for spinal cord injury underscores that therapy frequency, duration, and progression remain heterogeneous, complicating comparisons and masking device-specific benefits [26]. Complementarily, broad surveys of lower-limb exoskeletons and of biomechanical models emphasize the need for unified evaluation

ISSN 2306-5478

metrics and simulation pipelines that bridge mechanism design with human outcome measures [27]. These gaps reinforce the value of analyses that start from task biomechanics (e.g., STS) and propagate through kinematics, internal/external loads, and structural checks to inform parameter choices (geometry, stiffness/damping, pretension) for specific device sections like pelvis-foot [28].

In summary, prior literature establishes: 1) STS places large, speed-sensitive demands on hip-knee extensors and requires coordinated trunk and ankle strategies; 2) passive/quasi-passive elements can beneficially redistribute effort when their torque-angle behavior matches task kinematics; 3) HDI – especially pelvis–hip alignment and distal foot mechanics – critically determines comfort and internal load paths. However, only few studies isolate the pelvis-foot section as the design unit of analysis, linking its geometry and passive module parameters to STS kinematics, joint reactions, and member stresses in an integrated way. The present paper addresses this gap by deriving and validating a kinematic-force model of the pelvis-foot segment of a passive lower-limb exoskeleton and using it to map design parameters to motion trajectories and load distributions that are relevant for rehabilitation scenarios.

3. Research Methodology. The layout of the pelvis-foot section proposed in this study is shown in Fig. 1. The user's footwear is rigidly secured to the exoskeleton foot, which consists of a forefoot segment 1 and a hindfoot segment 2 interconnected by a cylindrical hinge 3. The foot contacts the support surface via a rubber outsole 4. Through a hinged (bearing) joint 5, which acts as the ankle joint, the stance foot is connected to the shank link 6. The angular setting of the foot relative to the shank link 6 is adjusted by a spring-damper unit 7. Via a hinged joint 8, functioning as the knee joint, the shank link 6 is connected to the thigh link 9. Their mutual angular position is regulated by a spring-damper unit 10. The thigh link 9 is pivoted to the pelvic plate 11 by means of a bearing joint 12 that serves as the hip joint. The angular position of the thigh link 9 with respect to the pelvic plate 11 is adjusted by a spring-damper unit 7. Each leg is rigidly affixed to the corresponding exoskeleton elements by four straps 14, and the pelvic plate 11 is firmly fastened to the user's torso by a strap 15.

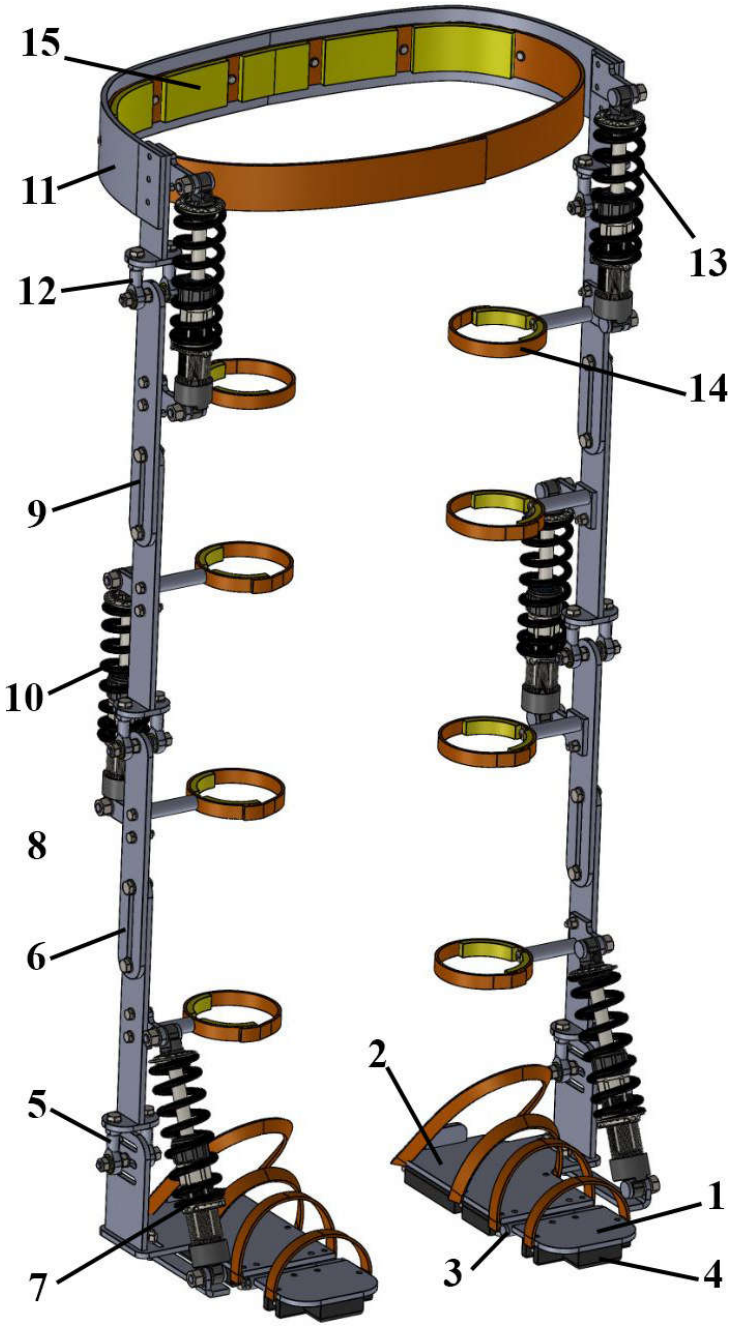

Fig. 1. Proposed layout of the pelvis–foot section of the exoskeleton

In the nominal (unloaded) configuration, spring–damper unit 10 ensures parallel alignment of the shank link 6 and the thigh link 9, whereas unit 13 holds link 9 perpendicular to the mounting plane of the pelvic plate 11. In the unloaded state, the exoskeleton foot is preset at an obtuse angle (120–140°) relative to the shank link 6. During upright stance, the spring of unit 7 is compressed; during stepping, the potential energy stored in this elastic unit is released to assist the user in taking a step. The spring–damper units 13 and 14 (Fig. 1) are employed during

 ISSN 2306-5478

sit-to-stand and stand-to-sit maneuvers. The potential energy accumulated through compression of the respective springs while squatting is released on rising, thereby reducing the muscular load.

According to the proposed design of the pelvis-foot section of the exoskeleton, both spatial and planar kinematic schemes were developed (Fig. 2). The spatial scheme (Fig. 2, a) can be used to describe the exoskeleton's stepping (gait) process, whereas the planar scheme (Fig. 2, b) is intended for analyzing stand-to-sit and sit-to-stand maneuvers.

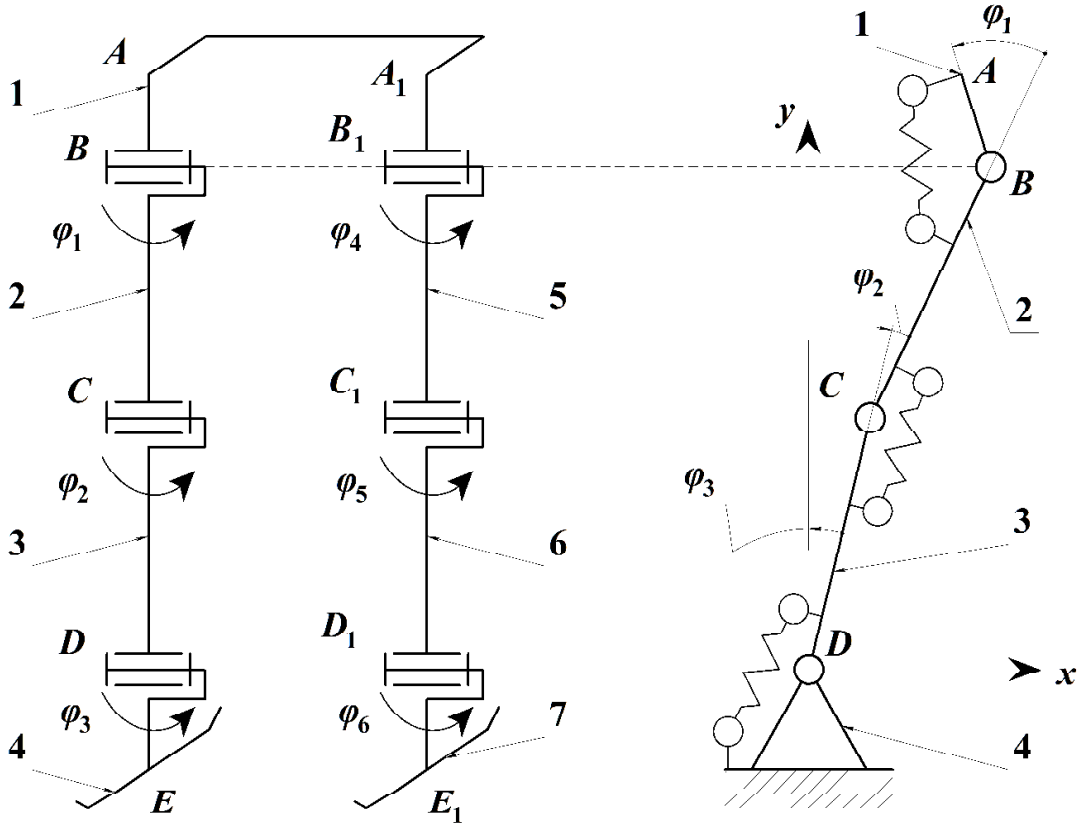

Fig. 2. Spatial and planar kinematic schemes of the exoskeleton

When considering sit-to-stand/stand-to-sit with the exoskeleton feet 4 and 7 in contact with the support surface, each leg is modeled as an open kinematic chain (a revolute-link mechanism) comprising three moving links (1–2–3) and three revolute joints (*B*, *C*, *D*) connecting these links. Links 1, 2, and 3 idealize the shank, thigh, and pelvic segments of the human skeleton, respectively, while joints *B*, *C*, and *D* represent the hip, knee, and ankle joints, respectively. In this context, spring–damper elements play the role of "passive muscles".

The overall number of degrees of freedom of the exoskeleton is six; however, for analyzing characteristic operating modes during sit-to-stand/stand-to-sit, it is sufficient to study a planar three-degree-of-freedom linkage that models the motion of one leg. As generalized coordinates, let us adopt the relative angular displacements φ_1, φ_2, and φ_3 of each subsequent link of the kinematic chain with respect to the preceding one (see Fig. 2, b).

As a representative operating mode of the exoskeleton, let us consider the human sit-to-stand/stand-to-sit transitions. For this purpose, let us use the simplified kinematic scheme of the exoskeleton shown in Fig. 2, b. Let us place the origin of the planar Cartesian coordinate system at point *D*, direct the *Dx* axis horizontally to the right, and the *Dy* axis vertically upward.

To determine the coordinates of point *C*, which undergoes rotational motion about the hinge at *D*, let us write the following equations:

$$x_C = l_{CD} \cdot \sin\varphi_3; \qquad y_C = l_{CD} \cdot \cos\varphi_3, \tag{1}$$

where l_{CD} is the length of the link *CD*.

Knowing that point *B* rotates about hinge *C* according to the law governed by the generalized coordinate φ_2, let us write the equations of motion for the exoskeleton's hip joint as:

$$\begin{aligned} x_B &= x_C + l_{BC} \cdot \sin(\varphi_2 + \varphi_3) = l_{CD} \cdot \sin\varphi_3 + l_{BC} \cdot \sin(\varphi_2 + \varphi_3); \\ y_B &= y_C + l_{BC} \cdot \cos(\varphi_2 + \varphi_3) = l_{CD} \cdot \cos\varphi_3 + l_{BC} \cdot \cos(\varphi_2 + \varphi_3), \end{aligned} \tag{2}$$

where l_{BC} is the length of the link *BC*.

Assuming that link *AB* models the position of the human trunk during sit-to-stand/stand-to-sit and taking into account the corresponding motion law φ_1, let us write the following equations to determine the coordinates of point *A*:

$$\begin{aligned} x_A &= x_B + l_{AB} \cdot \sin(\varphi_2 + \varphi_3 - \varphi_1) = l_{CD} \cdot \sin\varphi_3 + \\ &+ l_{BC} \cdot \sin(\varphi_2 + \varphi_3) + l_{AB} \cdot \sin(\varphi_2 + \varphi_3 - \varphi_1); \\ y_A &= y_B + l_{AB} \cdot \cos(\varphi_2 + \varphi_3 - \varphi_1) = l_{CD} \cdot \cos\varphi_3 + \\ &+ l_{BC} \cdot \cos(\varphi_2 + \varphi_3) + l_{AB} \cdot \cos(\varphi_2 + \varphi_3 - \varphi_1), \end{aligned} \tag{3}$$

where l_{AB} is the length of the link *AB*.

The laws governing the variation of the generalized coordinates φ_1, φ_2, and φ_3 in characteristic motions have been studied extensively

 ISSN 2306-5478

and are documented in numerous scientific and instructional works in biomechanics, human anatomy, osteology, and rehabilitative therapy (see, e.g., [4–9]).

4. Results and Discussion. To perform the numerical simulation of the exoskeleton's motion, let us specify its geometric parameters and the time laws of the generalized coordinates:

1) the geometric parameters are consistent with the developed exoskeleton layout (see Fig. 1): l_{AB} = 160 mm; l_{BC} = 500 mm; l_{AB} = 460 mm;

2) the motion laws are adopted in accordance with the findings reported in [4–9]:

$$\varphi_3(t) \approx \begin{cases} 0.06 \cdot \pi \cdot t, \text{ if } 0 \le t \le 1.5 \text{ s}, \\ 0.09 \cdot \pi, \text{ if } 1.5 \text{ s} \le t \le 2 \text{ s}; \end{cases}$$

$$\varphi_2(t) \approx \begin{cases} 0.25 \cdot \pi \cdot t, \text{ if } 0 \le t \le 1.5 \text{ s}, \\ 0.375 \cdot \pi, \text{ if } 1.5 \text{ s} \le t \le 2 \text{ s}; \end{cases} \quad (4)$$

$$\varphi_1(t) \approx \begin{cases} 0.4 \cdot \pi \cdot t, \text{ if } 0 \le t \le 1.5 \text{ s}, \\ 0.6 \cdot \pi - 0.3 \cdot \pi \cdot (t - 1.5), \text{ if } 1.5 \text{ s} \le t \le 2 \text{ s}. \end{cases}$$

A sample software implementation of the exoskeleton's squatting algorithm in the Mathcad environment is presented in Fig. 3.

Based on the numerical simulation results for the exoskeleton's squatting process (Fig. 3), the following conclusions can be drawn. The knee joint *C* travels along a circular trajectory (red line) about the ankle *D* (the origin of coordinates). The hip joint *B* follows a quasi-elliptic trajectory (blue line). Superposition of two rotations produces an ellipse-like trajectory whose curvature decreases as the thigh approaches the seated configuration. During squatting, the exoskeleton's trunk initially leans slightly forward and, once a seated configuration is reached, returns to an upright posture (green line).

$$lAB := 160 \qquad lBC := 500 \qquad lCD := 460$$

$$\varphi 3(t) := \begin{cases} 0.06\cdot\pi\cdot t & \text{if } 0 \le t \le 1.5 \\ 0.09\cdot\pi & \text{if } 1.5 < t \le 2 \end{cases}$$

$$\varphi 2(t) := \begin{cases} 0.25\cdot\pi\cdot t & \text{if } 0 \le t \le 1.5 \\ 0.375\cdot\pi & \text{if } 1.5 \le t \le 2 \end{cases} \qquad \varphi 1(t) := \begin{cases} 0.4\cdot\pi\cdot t & \text{if } 0 \le t \le 1.5 \\ 0.6\cdot\pi - 0.3\cdot\pi\cdot(t-1.5) & \text{if } 1.5 \le t \le 2 \end{cases}$$

$$xC(t) := lCD\cdot\sin(\varphi 3(t)) \qquad yC(t) := lCD\cdot\cos(\varphi 3(t))$$

$$xB(t) := xC(t) + lBC\cdot\sin(\varphi 2(t) + \varphi 3(t)) \qquad yB(t) := yC(t) + lBC\cdot\cos(\varphi 2(t) + \varphi 3(t))$$

$$xA(t) := xB(t) + lAB\cdot\sin(\varphi 2(t) + \varphi 3(t) - \varphi 1(t)) \qquad yA(t) := yB(t) + lAB\cdot\cos(\varphi 2(t) + \varphi 3(t) - \varphi 1(t))$$

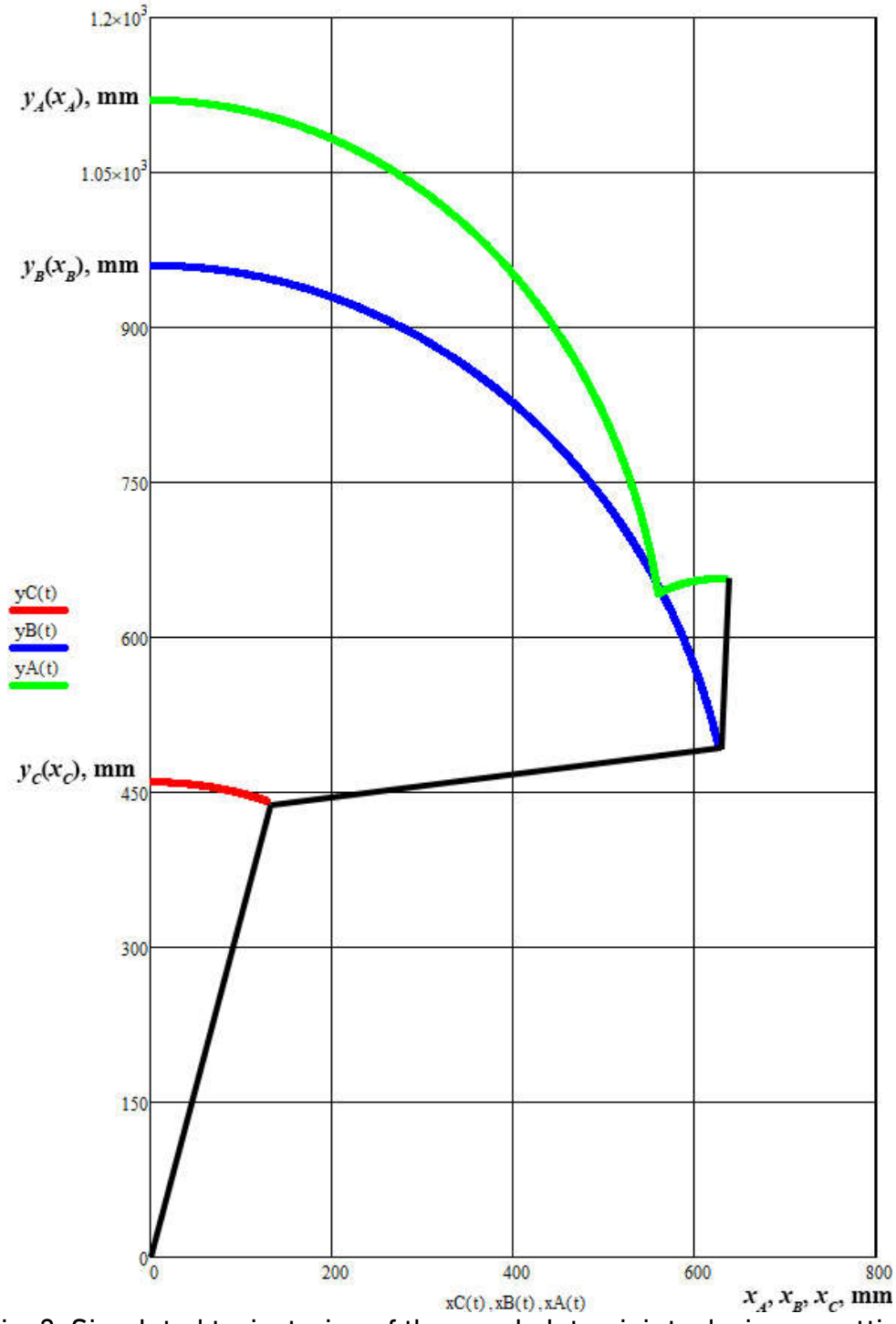

Fig. 3. Simulated trajectories of the exoskeleton joints during squatting

 ISSN 2306-5478

To assess the adequacy of the analytically obtained results, we develop a simulation model (Fig. 4) of the exoskeleton mechanism in the MapleSim software package, which is currently among the leading platforms for automated modeling and engineering analysis of a wide range of physical systems.

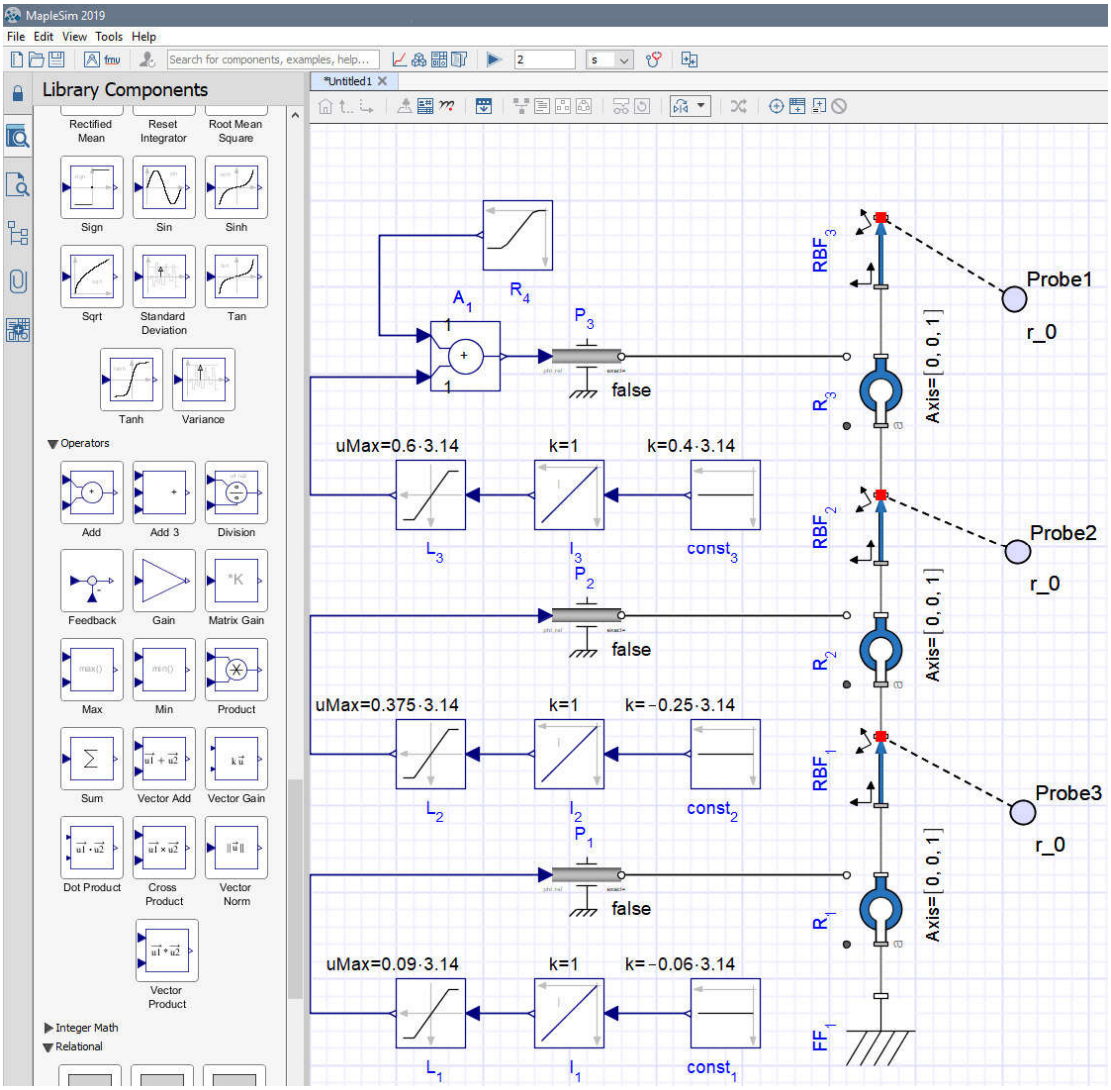

Fig. 4. Simulation model of the exoskeleton mechanical system developed in MapleSim software

By prescribing the same geometric parameters of the exoskeleton's mechanical system and the time laws of the generalized coordinates as in the mathematical modeling, its motion was simulated. The resulting trajectories of the knee and hip joints, as well as of the exoskeleton trunk, are presented in Fig. 5.

Based on the simulation results (Fig. 5) and comparing them with the results of mathematical modeling (see Fig. 3), we can conclude that

the proposed analytical relations (1)–(3) adequately describe the motion of the exoskeleton's mechanical system.

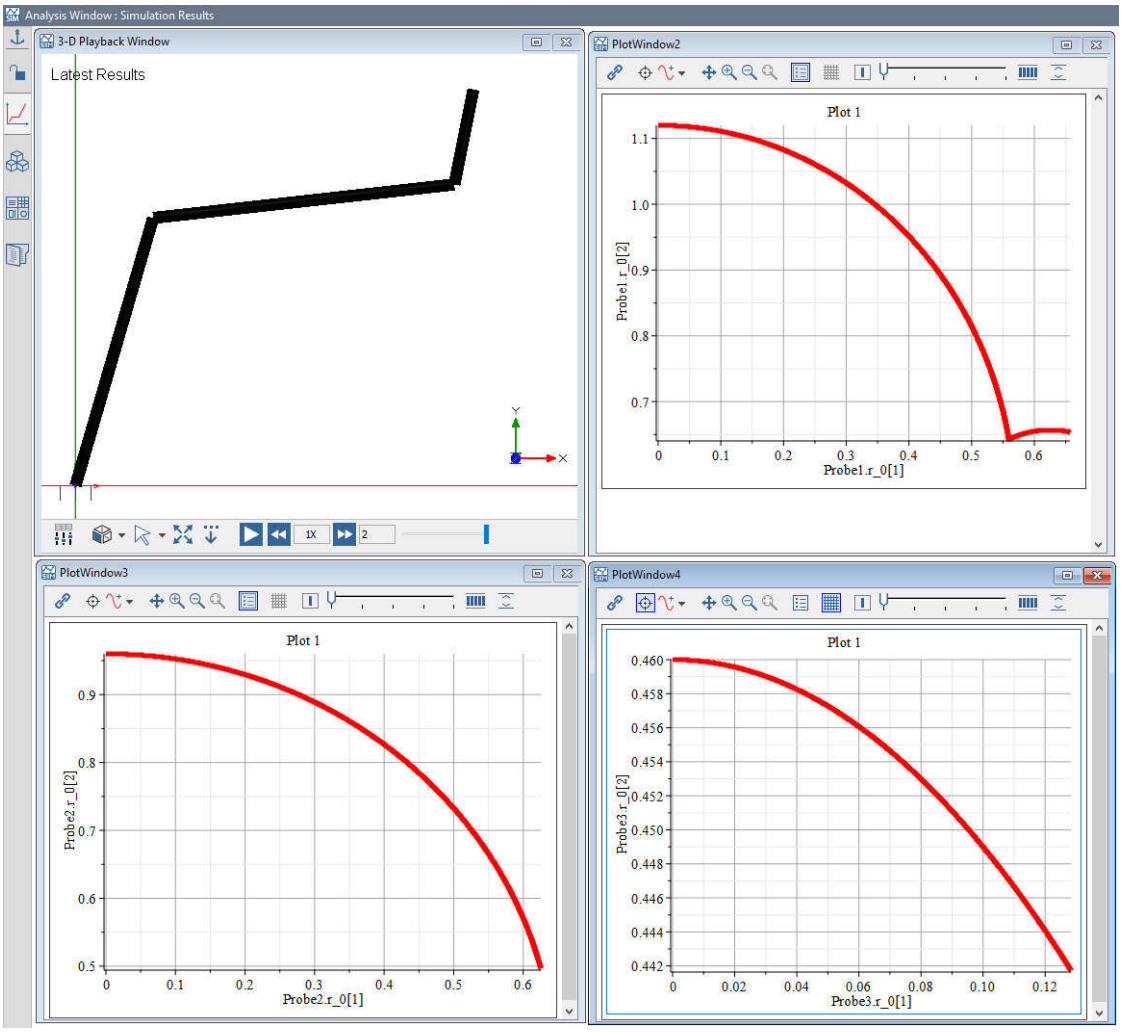

Fig. 5. Simulation results for the motion of the exoskeleton's pelvis-foot section during squatting

Let us consider the loading schemes in which the exoskeleton is subjected to a vertical static force (Fig. 2.6) equal to the maximum body weight of the intended user. In this study, we assume this force does not exceed 1500 N. With sufficient accuracy, the point of application of this force may be taken as point *A* on the exoskeleton's pelvic plate 1. In the upright configuration of the exoskeleton (Fig. 6, a), the axial compressive forces in each link (thigh, shank, etc.) are equal to the body weight supported by a single leg, while the contralateral leg is lifted or taking a step. In this case, the links must be verified for bearing (crushing) stresses at the pin-joint interfaces and for stiffness.

 ISSN 2306-5478

During the sitting-down phase, the axial compressive force gradually transitions into a bending load (Fig. 6, b). The bending moment attains its maximum when the thigh link 2 is in the horizontal position:

$$M_{b.\max} \approx F \cdot l_{BC} = 1500 \cdot 0.5 = 750 \text{ N} \cdot \text{m}. \quad (5)$$

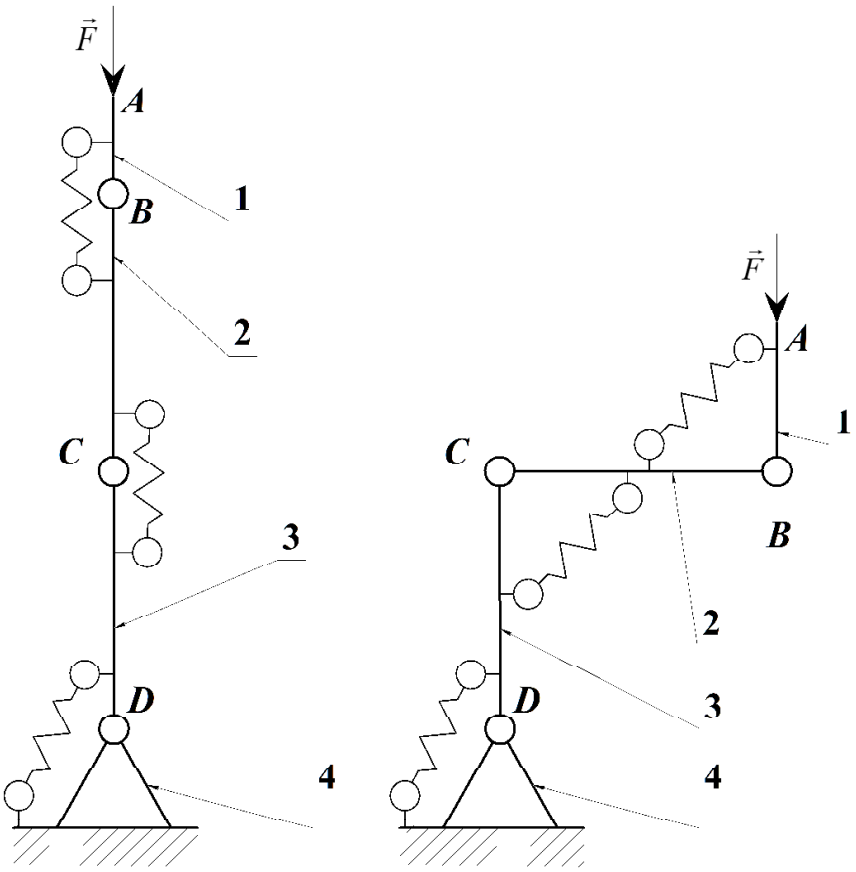

Fig. 6. Simplified loading schematics of the exoskeleton

In the next stage of the study, let us perform a simulation of the stress-strain state of the thigh link in SolidWorks Simulation software using the finite element method (FEM). Let us consider the case in which the link is subjected to a maximum load with a magnitude of 1500 N in the seated and standing configurations of the exoskeleton.

The computational three-dimensional model of the exoskeleton's thigh link is shown in Fig. 7. One end of the link is rigidly constrained, while the other is loaded by two oppositely directed forces that emulate the upright (standing) and horizontal (seated) configurations of the exoskeleton. For the simulation, the part must be discretized into a finite number of elements; that is, a mesh must be generated in SolidWorks Simulation software (Fig. 8). Running the analysis yields contour plots of equivalent stress and strain for the thigh link.

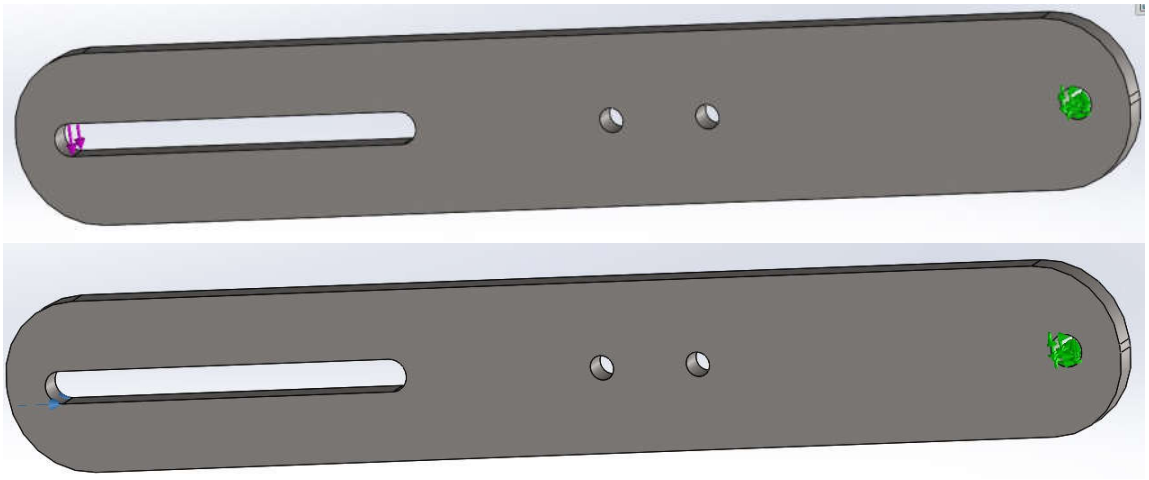

Fig. 7. Simulation loading model of the exoskeleton's thigh link

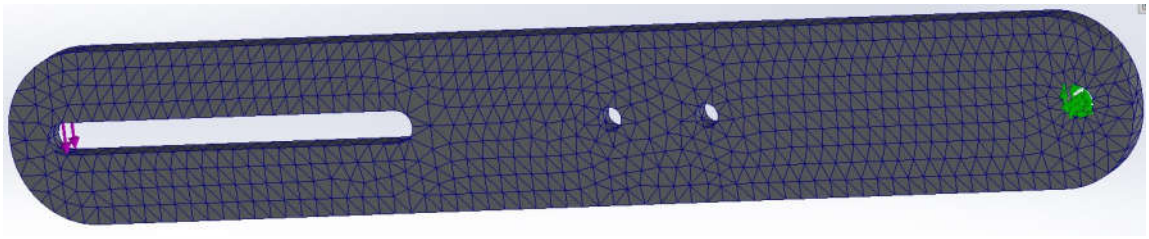

Fig. 8. Finite element mesh

A linear-elastic, isotropic FEM was run in SolidWorks Simulation for the thigh link with one end fully constrained and the opposite end loaded to emulate the bending case representative of the seated configuration and the axial compression case representative of the upright configuration. Second-order tetra elements and curvature-based meshing were used around holes/slots (stress raisers).

In the bending case (Fig. 9, *a*), the maximum equivalent (von Mises) stress is approximately 154 MPa, localized at the geometric discontinuities near the slot/fastener holes at the loaded end (classical notch effect). The stress field decays rapidly away from these features, indicating section-modulus driven bending with local concentration dominating the peak. Relative to the material yield strength noted in the legend (220 MPa), the utilization is about 70% (safety factor is almost 1.43). If a conservative allowable stress of 160 MPa (e.g., for steel St. 3) is adopted, the margin is approximately 4%, i.e., barely acceptable without further optimization.

In the compression case (Fig. 9, *b*), the peak stress is about 26–27 MPa, concentrated at the fillet/slot root where load enters the section. This is less than 15% of yield, with ample static margin; buckling is not triggered in this local, short-link configuration.

ISSN 2306-5478

a)

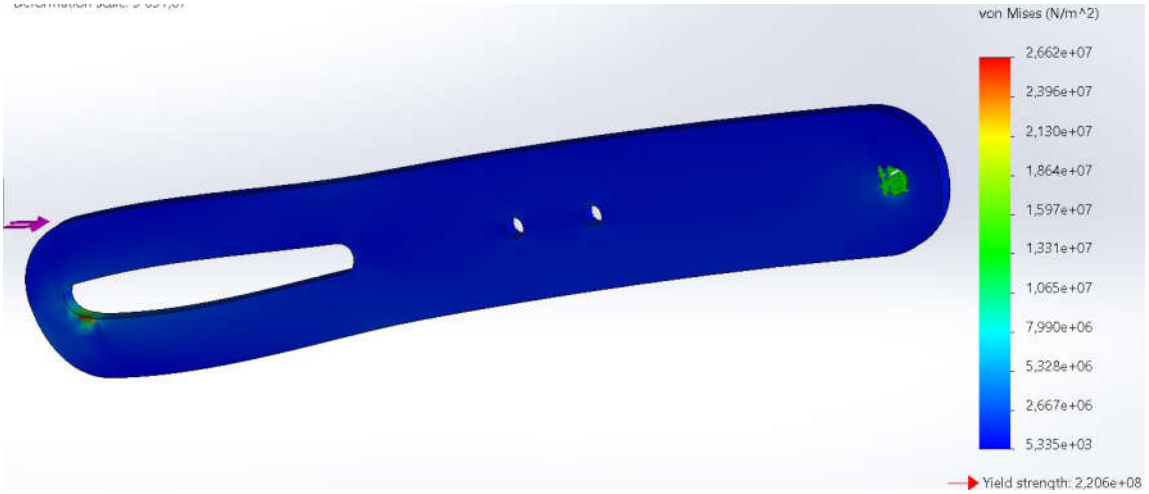

b)

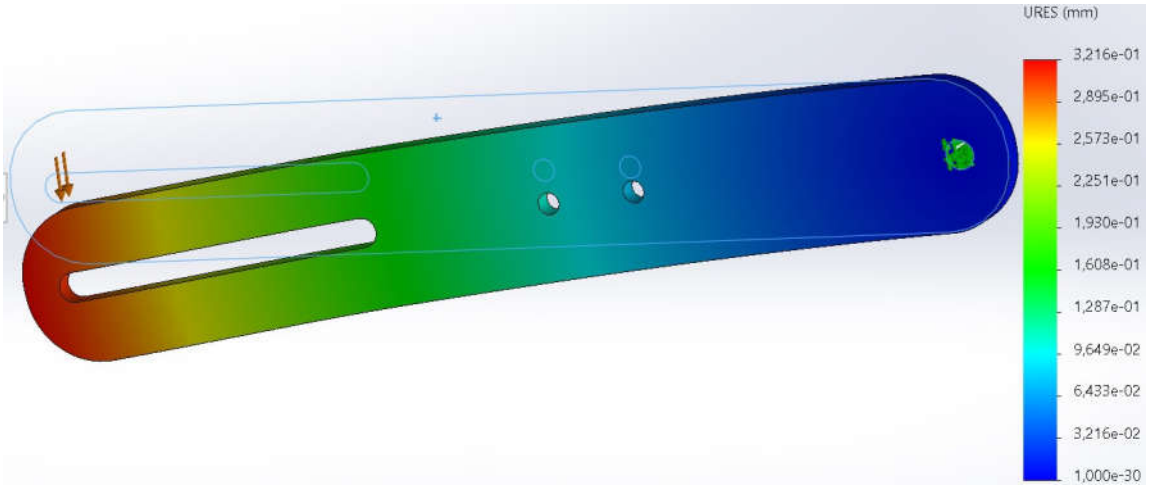

c)

Fig. 9. Results of simulation of the stress-strain state of the exoskeleton's thigh link: *a* – contour plot of the equivalent stress under link bending; *b* – contour plot of the equivalent stress under link compression; *c* – deflection plot for the link in bending

Considering the deflection in bending (Fig. 9, *c*), the maximum tip deflection is about 0.3–0.32 mm, with a smooth gradient along the span and the largest displacement at the loaded end. From a human-device interaction perspective, that magnitude is typically small relative to joint-alignment tolerances; however, if your hip/knee alignment budget is less than ±0.5 mm, the link satisfies a practical stiffness criterion for the examined load.

5. Conclusions. This work formulated and validated a compact modeling pipeline for the pelvis-foot section of a passive lower-limb exoskeleton, combining a closed-vector-loop planar model (three generalized coordinates) with multibody verification and structural checks. The approach reliably captures sit-to-stand/stand-to-sit (STS) kinematics and loads and can serve as a design aid for section-level decisions.

The derived motion laws reproduce physiologically plausible loci: the knee travels on a near-circular arc about the ankle, the hip follows a quasi-elliptic path, and the trunk executes a controlled lean-and-recovery. Agreement between Mathcad trajectories and MapleSim multibody results confirms the adequacy of the analytical relations (1)–(3) for STS analysis.

A simplified loading framework linked user mass to section loads and showed that during sitting the axial load transitions into dominant bending, with the thigh link experiencing a peak bending moment of approximately 750 N·m in the horizontal position. This isolates the thigh link as a critical structural member for design checks.

Finite-element analysis of the thigh link under a design load up to 1.5 kN yielded a maximum von Mises stress of about 154 MPa at geometric stress raisers and a maximum tip deflection of approximately 0.3–0.32 mm. Against a reference yield strength of 220 MPa (for steel St. 3), the safety factor is about 1.43; relative to a conservative allowable of 160 MPa, the margin is narrow but acceptable. Compression loads produced low stresses (about 26–27 MPa) with ample reserve.

These findings indicate that the proposed architecture and parameterization of the spring-damper units are sufficient to assist STS while keeping stresses and deformations within acceptable bounds for the examined materials and loads – supporting feasibility for passive assistance without actuators.

Design guidance emerging from the analysis includes: prioritizing stress-concentration mitigation near slots/holes (fillets, generous radii,

 ISSN 2306-5478

load distribution at interfaces), modest section-modulus increases (local thickness/width) if higher margins are desired, and progressive damping at the hip module to smooth the end-of-descent transition; alternatively, higher-yield steels can raise reserves without mass growth.

Limitations of the present study include the planar approximation for STS, linear-elastic FEA without fatigue/buckling durability, simplified boundary conditions at joints/straps, and the absence of human-subject tests. Future work should extend to 3-D misalignment effects, contact/friction modeling at joints and footwear, parameter optimization of spring-damper units (stiffness, pretension, damping) for subject-specific anthropometrics, fatigue life and buckling checks, and experimental validation with instrumented trials.

1. Rodríguez-Fernández A., Lobo-Prat J., Font-Llagunes J. M. Systematic review on wearable lower-limb exoskeletons for gait training in neuromuscular impairments. *Journal of NeuroEngineering and Rehabilitation*. 2021. Vol. 18(1). P. 22. URL: https://doi.org/10.1186/s12984-021-00815-5 **2.** Nepomuceno P., Souza W. H., Pakosh M., Musselman K. E., Craven B. C. Exoskeleton-based exercises for overground gait and balance rehabilitation in spinal cord injury: a systematic review of dose and dosage parameters. *Journal of NeuroEngineering and Rehabilitation*. 2024. Vol. 21(1). P. 73. URL: https://doi.org/10.1186/s12984-024-01365-2 **3.** Baud R., Manzoori A. R., Ijspeert A., Bouri M. Review of control strategies for lower-limb exoskeletons to assist gait. *Journal of NeuroEngineering and Rehabilitation*. 2021. Vol. 18(1). P. 119. URL: https://doi.org/10.1186/s12984-021-00906-3 **4.** Pai Y. C., Rogers M. W. Speed variation and resultant joint torques during sit-to-stand. *Archives of Physical Medicine and Rehabilitation*. 1991. Vol. 72(11). Pp. 881–885. URL: https://doi.org/10.1016/0003-9993(91)90004-3 **5.** Janssen W. G. M., Bussmann H. B. J., Stam H. J. Determinants of the sit-to-stand movement: a review. *Physical Therapy*. 2002. Vol. 82(9). Pp. 866–879. URL: https://doi.org/10.1093/ptj/82.9.866 **6.** Baer G. D., Ashburn A. M. Trunk movements in older subjects during sit-to-stand. Archives of Physical Medicine and Rehabilitation. 1995. Vol. 76(9). Pp. 844–849. URL: https://doi.org/10.1016/S0003-9993(95)80550-8 **7.** Pourahmadi M. R., Ebrahimi Takamjani I., Jaberzadeh S., Sarrafzadeh J., Sanjari M. A., Bagheri R., Taghipour M. Kinematics of the spine during sit-to-stand movement using motion analysis systems: a systematic review of literature. *Journal of Sport Rehabilitation*. 2019. Vol. 28(1). Pp. 77–93. URL: https://doi.org/10.1123/jsr.2017-0147 **8.** Abujaber S. B., Marmon A. R., Pozzi F., Rubano J. J., Zeni J. A. Jr. Sit-to-stand biomechanics before and after total hip arthroplasty. *The Journal of Arthroplasty*. 2015. Vol. 30(11). Pp. 2027–2033. URL: https://doi.org/10.1016/j.arth.2015.05.024 **9.** Li J., Xue Q., Yang S., Han X., Zhang S., Li M., Guo J. Kinematic analysis of the human body during sit-to-stand in healthy young adults. *Medicine (Baltimore)*. 2021. Vol. 100(22). P. e26208. URL: https://doi.org/10.1097/MD.0000000000026208 **10.** Sadeh S., Gobert D., Shen K.-H., Foroughi F., Hsiao H.-Y. Biomechanical and neuromuscular control characteristics of sit-to-stand transfer in young and older adults: a systematic review with implications for balance regulation mechanisms. *Clinical Biomechanics*. 2023. Vol. 109. P. 106068.

URL: https://doi.org/10.1016/j.clinbiomech.2023.106068 **11.** Bryan G. M., Franks P. W., Song S., Voloshina A. S., Reyes R., O'Donovan M. P., Gregorczyk K. N., Collins S. H. Optimized hip–knee–ankle exoskeleton assistance at a range of walking speeds. *Journal of NeuroEngineering and Rehabilitation*. 2021. Vol. 18. P. 152. URL: https://doi.org/10.1186/s12984-021-00943-y **12.** Galle S., Malcolm P., Collins S. H., De Clercq D. Reducing the metabolic cost of walking with an ankle exoskeleton: interaction between actuation timing and power. *Journal of NeuroEngineering and Rehabilitation*. 2017. Vol. 14. P. 35. URL: https://doi.org/10.1186/s12984-017-0235-0 **13.** Tang X., Wang X., Ji X., Zhou Y., Yang J., Wei Y., Zhang W. A wearable lower limb exoskeleton: reducing the energy cost of human movement. *Micromachines*. 2022. Vol. 13(6). P. 900. URL: https://doi.org/10.3390/mi13060900 **14.** Lovrenovic Z., Doumit M. Development and testing of a passive walking assist exoskeleton. *Biocybernetics and Biomedical Engineering*. 2019. Vol. 39(4). Pp. 992–1004. URL: https://doi.org/10.1016/j.bbe.2019.01.002 **15.** Washabaugh E. P., Augenstein T. E., Ebenhoeh A. M., Qiu J., Ford K. A., Krishnan C. Design and preliminary assessment of a passive elastic leg exoskeleton for resistive gait rehabilitation. *IEEE Transactions on Biomedical Engineering*. 2021. Vol. 68(6). Pp. 1941–1950. URL: https://doi.org/10.1109/TBME.2020.3038582 **16.** Lee H., Kim S. H., Park H.-S. A fully soft and passive assistive device to lower the metabolic cost of sit-to-stand. *Frontiers in Bioengineering and Biotechnology*. 2020. Vol. 8. P. 966. URL: https://doi.org/10.3389/fbioe.2020.00966 **17.** Lindemann U., Krespach J., Daub U., Schneider M., Sczuka K. S., Klenk J. Effect of a passive exosuit on sit-to-stand performance in geriatric patients measured by body-worn sensors – a pilot study. *Sensors*. 2023. Vol. 23(2). P. 1032. URL: https://doi.org/10.3390/s23021032 **18.** Soni V., Vaz A. Kinematics and kinetics of a knee assistance exoskeleton for sit-to-stand and stand-to-sit motions with energy storage and regeneration: a bond graph approach. *Mechanism and Machine Theory*. 2025. Vol. 205. P. 105866. URL: https://doi.org/10.1016/j.mechmachtheory.2024.105866 **19.** Näf M. B., Junius K., Rossini M., Rodriguez-Guerrero C., Vanderborght B., Lefeber D. Misalignment compensation for full human-exoskeleton kinematic compatibility: state of the art and evaluation. *Applied Mechanics Reviews*. 2018. Vol. 70(5). P. 050802. URL: https://doi.org/10.1115/1.4042523 **20.** Bessler-Etten J., Schaake L., Prange-Lasonder G. B., Buurke J. H. Assessing effects of exoskeleton misalignment on knee joint load during swing using an instrumented leg simulator. *Journal of NeuroEngineering and Rehabilitation*. 2022. Vol. 19(1). P. 13. URL: https://doi.org/10.1186/s12984-022-00990-z **21.** Junius K., Degelaen M., Lefeber N., Swinnen E., Vanderborght B., Lefeber D. Bilateral, misalignment-compensating, full-DOF hip exoskeleton: design and kinematic validation. *Applied Bionics and Biomechanics*. 2017. Vol. 2017. P. 5813154. URL: https://doi.org/10.1155/2017/5813154 **22.** Wang Y., Wu X., Fang Y., Osawa K., Nakagawa K., Yamasaki S., Tanaka E. Design, control, and analysis of a 3-degree-of-freedom kinematic–biologically matched hip joint structure for lower limb exoskeleton. *Machines*. 2024. Vol. 12(12). P. 924. URL: https://doi.org/10.3390/machines12120924 **23.** Yang X., Guo S., Wang P., Wu Y., Niu L., Liu D. Design and optimization analysis of an adaptive knee exoskeleton. *Chinese Journal of Mechanical Engineering*. 2024. Vol. 37. P. 104. URL: https://doi.org/10.1186/s10033-024-01084-8 **24.** Zhang X., Liu Y.-X., Wang R., Gutierrez-Farewik E. M. Soft ankle exoskeleton to counteract dropfoot and excessive inversion. *Frontiers in Neurorobotics*. 2024. Vol. 18. P. 1372763. URL:

 ISSN 2306-5478

https://doi.org/10.3389/fnbot.2024.1372763 **25.** Antonellis P., Galle S., De Clercq D., Malcolm P. Altering gait variability with an ankle exoskeleton. *PLoS ONE*. 2018. Vol. 13(10). P. e0205088. URL: https://doi.org/10.1371/journal.pone.0205088 **26.** Nepomuceno P., Souza W. H., Pakosh M., Musselman K. E., Craven B. C. Exoskeleton-based exercises for overground gait and balance rehabilitation in spinal cord injury: a systematic review of dose and dosage parameters. *Journal of NeuroEngineering and Rehabilitation*. 2024. Vol. 21(1). P. 73. URL: https://doi.org/10.1186/s12984-024-01365-2 **27.** Rodríguez-Fernández A., Lobo-Prat J., Font-Llagunes J. M. Systematic review on wearable lower-limb exoskeletons for gait training in neuromuscular impairments. *Journal of NeuroEngineering and Rehabilitation*. 2021. Vol. 18(1). P. 22. URL: https://doi.org/10.1186/s12984-021-00815-5 **28.** Firouzi V., Seyfarth A., Song S., von Stryk O., Sharbafi M. A. Biomechanical models in the lower-limb exoskeletons development: a review. *Journal of NeuroEngineering and Rehabilitation*. 2025. Vol. 22(1). P. 12. URL: https://doi.org/10.1186/s12984-025-01556-5

REFERENCES:

1. Rodríguez-Fernández A., Lobo-Prat J., Font-Llagunes J. M. Systematic review on wearable lower-limb exoskeletons for gait training in neuromuscular impairments. *Journal of NeuroEngineering and Rehabilitation*. 2021. Vol. 18(1). P. 22. URL: https://doi.org/10.1186/s12984-021-00815-5 **2.** Nepomuceno P., Souza W. H., Pakosh M., Musselman K. E., Craven B. C. Exoskeleton-based exercises for overground gait and balance rehabilitation in spinal cord injury: a systematic review of dose and dosage parameters. *Journal of NeuroEngineering and Rehabilitation*. 2024. Vol. 21(1). P. 73. URL: https://doi.org/10.1186/s12984-024-01365-2 **3.** Baud R., Manzoori A. R., Ijspeert A., Bouri M. Review of control strategies for lower-limb exoskeletons to assist gait. *Journal of NeuroEngineering and Rehabilitation*. 2021. Vol. 18(1). P. 119. URL: https://doi.org/10.1186/s12984-021-00906-3 **4.** Pai Y. C., Rogers M. W. Speed variation and resultant joint torques during sit-to-stand. *Archives of Physical Medicine and Rehabilitation*. 1991. Vol. 72(11). Pp. 881–885. URL: https://doi.org/10.1016/0003-9993(91)90004-3 **5.** Janssen W. G. M., Bussmann H. B. J., Stam H. J. Determinants of the sit-to-stand movement: a review. *Physical Therapy*. 2002. Vol. 82(9). Pp. 866–879. URL: https://doi.org/10.1093/ptj/82.9.866 **6.** Baer G. D., Ashburn A. M. Trunk movements in older subjects during sit-to-stand. Archives of Physical Medicine and Rehabilitation. 1995. Vol. 76(9). Pp. 844–849. URL: https://doi.org/10.1016/S0003-9993(95)80550-8 **7.** Pourahmadi M. R., Ebrahimi Takamjani I., Jaberzadeh S., Sarrafzadeh J., Sanjari M. A., Bagheri R., Taghipour M. Kinematics of the spine during sit-to-stand movement using motion analysis systems: a systematic review of literature. *Journal of Sport Rehabilitation*. 2019. Vol. 28(1). Pp. 77–93. URL: https://doi.org/10.1123/jsr.2017-0147 **8.** Abujaber S. B., Marmon A. R., Pozzi F., Rubano J. J., Zeni J. A. Jr. Sit-to-stand biomechanics before and after total hip arthroplasty. *The Journal of Arthroplasty*. 2015. Vol. 30(11). Pp. 2027–2033. URL: https://doi.org/10.1016/j.arth.2015.05.024 **9.** Li J., Xue Q., Yang S., Han X., Zhang S., Li M., Guo J. Kinematic analysis of the human body during sit-to-stand in healthy young adults. *Medicine (Baltimore)*. 2021. Vol. 100(22). P. e26208. URL: https://doi.org/10.1097/MD.0000000000026208 **10.** Sadeh S., Gobert D., Shen K.-H., Foroughi F., Hsiao H.-Y. Biomechanical and neuromuscular control characteristics of sit-to-stand transfer in young and older adults: a systematic review with implications

for balance regulation mechanisms. *Clinical Biomechanics*. 2023. Vol. 109. P. 106068. URL: https://doi.org/10.1016/j.clinbiomech.2023.106068 **11.** Bryan G. M., Franks P. W., Song S., Voloshina A. S., Reyes R., O'Donovan M. P., Gregorczyk K. N., Collins S. H. Optimized hip–knee–ankle exoskeleton assistance at a range of walking speeds. *Journal of NeuroEngineering and Rehabilitation*. 2021. Vol. 18. P. 152. URL: https://doi.org/10.1186/s12984-021-00943-y **12.** Galle S., Malcolm P., Collins S. H., De Clercq D. Reducing the metabolic cost of walking with an ankle exoskeleton: interaction between actuation timing and power. *Journal of NeuroEngineering and Rehabilitation*. 2017. Vol. 14. P. 35. URL: https://doi.org/10.1186/s12984-017-0235-0 **13.** Tang X., Wang X., Ji X., Zhou Y., Yang J., Wei Y., Zhang W. A wearable lower limb exoskeleton: reducing the energy cost of human movement. *Micromachines*. 2022. Vol. 13(6). P. 900. URL: https://doi.org/10.3390/mi13060900 **14.** Lovrenovic Z., Doumit M. Development and testing of a passive walking assist exoskeleton. *Biocybernetics and Biomedical Engineering*. 2019. Vol. 39(4). Pp. 992–1004. URL: https://doi.org/10.1016/j.bbe.2019.01.002 **15.** Washabaugh E. P., Augenstein T. E., Ebenhoeh A. M., Qiu J., Ford K. A., Krishnan C. Design and preliminary assessment of a passive elastic leg exoskeleton for resistive gait rehabilitation. *IEEE Transactions on Biomedical Engineering*. 2021. Vol. 68(6). Pp. 1941–1950. URL: https://doi.org/10.1109/TBME.2020.3038582 **16.** Lee H., Kim S. H., Park H.-S. A fully soft and passive assistive device to lower the metabolic cost of sit-to-stand. *Frontiers in Bioengineering and Biotechnology*. 2020. Vol. 8. P. 966. URL: https://doi.org/10.3389/fbioe.2020.00966 **17.** Lindemann U., Krespach J., Daub U., Schneider M., Sczuka K. S., Klenk J. Effect of a passive exosuit on sit-to-stand performance in geriatric patients measured by body-worn sensors – a pilot study. *Sensors*. 2023. Vol. 23(2). P. 1032. URL: https://doi.org/10.3390/s23021032 **18.** Soni V., Vaz A. Kinematics and kinetics of a knee assistance exoskeleton for sit-to-stand and stand-to-sit motions with energy storage and regeneration: a bond graph approach. *Mechanism and Machine Theory*. 2025. Vol. 205. P. 105866. URL: https://doi.org/10.1016/j.mechmachtheory.2024.105866 **19.** Näf M. B., Junius K., Rossini M., Rodriguez-Guerrero C., Vanderborght B., Lefeber D. Misalignment compensation for full human-exoskeleton kinematic compatibility: state of the art and evaluation. *Applied Mechanics Reviews*. 2018. Vol. 70(5). P. 050802. URL: https://doi.org/10.1115/1.4042523 **20.** Bessler-Etten J., Schaake L., Prange-Lasonder G. B., Buurke J. H. Assessing effects of exoskeleton misalignment on knee joint load during swing using an instrumented leg simulator. *Journal of NeuroEngineering and Rehabilitation*. 2022. Vol. 19(1). P. 13. URL: https://doi.org/10.1186/s12984-022-00990-z **21.** Junius K., Degelaen M., Lefeber N., Swinnen E., Vanderborght B., Lefeber D. Bilateral, misalignment-compensating, full-DOF hip exoskeleton: design and kinematic validation. *Applied Bionics and Biomechanics*. 2017. Vol. 2017. P. 5813154. URL: https://doi.org/10.1155/2017/5813154 **22.** Wang Y., Wu X., Fang Y., Osawa K., Nakagawa K., Yamasaki S., Tanaka E. Design, control, and analysis of a 3-degree-of-freedom kinematic–biologically matched hip joint structure for lower limb exoskeleton. *Machines*. 2024. Vol. 12(12). P. 924. URL: https://doi.org/10.3390/machines12120924 **23.** Yang X., Guo S., Wang P., Wu Y., Niu L., Liu D. Design and optimization analysis of an adaptive knee exoskeleton. *Chinese Journal of Mechanical Engineering*. 2024. Vol. 37. P. 104. URL: https://doi.org/10.1186/s10033-024-01084-8 **24.** Zhang X., Liu Y.-X., Wang R., Gutierrez-Farewik E. M. Soft ankle exoskeleton to counteract dropfoot and excessive

 ISSN 2306-5478

inversion. *Frontiers in Neurorobotics*. 2024. Vol. 18. P. 1372763. URL: https://doi.org/10.3389/fnbot.2024.1372763 **25.** Antonellis P., Galle S., De Clercq D., Malcolm P. Altering gait variability with an ankle exoskeleton. *PLoS ONE*. 2018. Vol. 13(10). P. e0205088. URL: https://doi.org/10.1371/journal.pone.0205088 **26.** Nepomuceno P., Souza W. H., Pakosh M., Musselman K. E., Craven B. C. Exoskeleton-based exercises for overground gait and balance rehabilitation in spinal cord injury: a systematic review of dose and dosage parameters. *Journal of NeuroEngineering and Rehabilitation*. 2024. Vol. 21(1). P. 73. URL: https://doi.org/10.1186/s12984-024-01365-2 **27.** Rodríguez-Fernández A., Lobo-Prat J., Font-Llagunes J. M. Systematic review on wearable lower-limb exoskeletons for gait training in neuromuscular impairments. *Journal of NeuroEngineering and Rehabilitation*. 2021. Vol. 18(1). P. 22. URL: https://doi.org/10.1186/s12984-021-00815-5 **28.** Firouzi V., Seyfarth A., Song S., von Stryk O., Sharbafi M. A. Biomechanical models in the lower-limb exoskeletons development: a review. *Journal of NeuroEngineering and Rehabilitation*. 2025. Vol. 22(1). P. 12. URL: https://doi.org/10.1186/s12984-025-01556-5

Тис М. А. [1; ORCID ID: 0009-0004-2208-9103],
аспірант,
Корендій В. М. [1; ORCID ID: 0000-0002-6025-3013],
к.т.н., доцент,
Маркович Б. М. [1; ORCID ID: 0000-0002-8813-9108],
д.ф.-м.н., професор,
Вишневський О. І. [1; ORCID ID: 0009-0006-7648-8630],
аспірант

[1]*Національний університет «Львівська політехніка», Львів, Україна*

КІНЕМАТИКО-СИЛОВИЙ АНАЛІЗ ТАЗОВО-СТОПОВОЇ ЧАСТИНИ ЕКЗОСКЕЛЕТА ДЛЯ РЕАБІЛІТАЦІЇ ЛЮДЕЙ З ПОРУШЕННЯМИ ОПОРНО-РУХОВОГО АПАРАТУ

У роботі виконано кінематико-силовий аналіз тазово-стопової частини пасивного нижньокінцівкового екзоскелета, призначеного для реабілітації осіб із порушеннями опорно-рухового апарату. Конструкція охоплює двосекційну стопу, з'єднану циліндричним шарніром, підп'ятник із гумовою підошвою, гомілковий і стегновий важелі, тазову пластину та енергоакумулювальні пружно-демпфувальні модулі в ділянках «щиколотка–коліно–таз». У ненавантаженому стані забезпечується квазіфізіологічна установка сегментів (зокрема, тупий кут стопи 120–140° відносно гомілкового важеля), а під час циклу «присідання–вставання» відбувається накопичення та контрольований вивід потенціальної енергії пружних елементів для зменшення пікових зусиль користувача. Кінематичне моделювання побудовано за методом замкнених векторних контурів для плоскої триланкової схеми з трьома

узагальненими координатами; чисельну реалізацію виконано в програмному продукті MathCad із двофазними часовими законами руху (загальна тривалість циклу 2 с). Для перевірки адекватності рівнянь руху створено імітаційну модель у програмному продукті MapleSim, за якою підтверджено характерні траєкторії: коловий шлях колінного суглоба відносно щиколотки, еліпсоподібний рух тазового суглоба та керований нахил-вирівнювання тулуба. Силовий аналіз включає розгляд вертикального статичного навантаження та перехід до згинального режиму при сіданні; виконавчий елемент – стегновий важіль – перевірено методом скінченних елементів у програмному продукті SolidWorks Simulation. Отримано максимум еквівалентних напружень на рівні близько 154 МПа та прогин, що не перевищує 0,3 мм, за розрахункового навантаження до 1,5 кН, що задовольняє умову міцності для сталі марки Ст. 3 (допустиме напруження близько 160 МПа). Узагальнено, що запропонована компоновка та параметризація пружно-демпфувальних вузлів є достатніми для асистування рухам «присідання–вставання» й можуть бути використані як основа для подальшої оптимізації під індивідуальні антропометричні дані і реабілітаційні протоколи.

Keywords: пасивний екзоскелет; реабілітація; кінематика; силовий аналіз; метод замкнутих векторних контурів; MathCad; MapleSim; SolidWorks Simulation; метод скінченних елементів; пружно-демпфувальний модуль; тазово-стоповий сегмент.

Отримано: 17 червня 2025 року
Прорецензовано: 02 вересня 2025 року
Прийнято до друку: 25 вересня 2025 року